Dynamics and Control of High Precision Magnetically Levitated Vibration Isolation Systems

K. Youcef-Toumi and T-J Yeh

Department of Mechanical Engineering
Massachusetts Institute of Technology

Mailing Address:
Kamal Youcef-Toumi
M.I.T. Room 35-233
77 Massachusetts Avenue
Cambridge, Massachusetts 02139
Telephone: (617) 253-2216

Abstract

Vibration control of flexible structures has received a great deal of interest in recent years. Several authors have investigated this topic in the areas of robot manipulators, space structures and flexible rotors . Key issues associated with the dynamics and control of vibration isolation systems are addressed in this paper.

Among other important issues to consider in the control of such systems, the location and number of actuators and sensors are essential to effectively control and suppress vibration. In this paper, we first address the selection of proper actuator and sensor locations leading to a controllable and observable system. The Rayleigh-Ritz modal analysis method is used to develop a lumped-parameter model of a flexible vibration isolation table top. This model is then used to investigate the system's controllability and observability including the coupling effects introduced by the magnetic bearing. This analysis results in necessary and sufficient conditions for proper selection of actuator and sensor locations. These locations are also important for both controller system's complexity and stability point of views. A favorable pole-zero plot of the open loop transfer functions is presented. Necessary and sufficient conditions for reducing the controller complexity are derived. The results are illustrated by examples using approximate mode shape functions.

Contents

1 Introduction

Sensitive instruments and precision machines have made it possible to investigate phenomena with dimensions of the nanometer scale. For example, current Michelson-type optical heterodyne interferometer can measure displacement with a resolution in the nanometer range [1]. Scanning Tunneling Microscopes (STM's) which use flexure linkage structures have Ångstrom resolution and range of motion on the order of one micron [2]. In these and other applications, vibration from ground motion and other distrubances, which may be in the micrometer level, will seriously degrade the overall system performance.

Traditional vibration isolation techniques can be generally divided into two categories: 1) passive and 2) active. Passive vibration isolation often involves the use of metal springs, elastomers, rubber, air springs or other passive elements to either absorb or dissipate vibration energy [3]. Passive techniques offer simple, inexpensive and reliable means to protect mechanical systems from environmental vibration. However, it is not possible for the passive vibration isolation methods to influence the system dynamics and adapt in real time. On the other hand, active vibration isolation techniques which use force generators that are adaptable to excitation and response characteristics of the system can actively counteract and cancel the undesirable vibration. In additiion, the active system provides significantly superior vibration isolation performance. The control force is often realized by pneumatic or electromechanical actuators. For example, Sandercock [4] proposed to combine both the active controlled electromechanical actuators and passive elastomers in building a dynamic antivibration system and has already become a commercialized product. In this system, the electromechanical actuators offer the damping force proportional to the absolute velocity of the table top while the elastomers provide the required compliance. This system is said to achieve $3\mu gs$ (3 mgal) RMS acceleration isolation performance [5].

In addition to the isolation of ground vibration, the suppression of induced vibration of work surface (or the table top plate) is also an important factor in vibration isolation system design. Since the table plate is not a perfect rigid body and thus considered flexible, the resonant frequencies of the table can be excited by the environmental disturbances such as acoustic noise, payload change, or the motion of a positioning system on the table top. In this case, the vibration modes of the table top will be excited and the performance of the system may degrade.

The use of actively controlled magnetic bearings is considered to not only achieve ultra high performance vibration isolation from the environment but also to suppress the induced vibration of the table top. Because of the unstable nature of the magnetic bearing, robust control scheme is needed to guarantee the performance. But prior to the control system design, the sensors and magnetic actuators should be properly located so that the vibration can be reduced effectively. As far as the flexibility of the top plate is concerned, this is related to the mode shapes of different vibration mode. This paper focuses on the actuator and sensor locations from the system controllability and observability points of view.

Controllability and observability of distributed systems has been investigated by Hughes and Skelton [6], and Yang and Mote [7]. In [6] the controllability and observability condition of linear matrix-second-order systems are discussed. But since the orthogonality of mode shape functions wasn't used, no direct relationship between the node line and the condition of controllability and observability is derived. In [7], although the locations of actuators and sensors were related to the modeshape functions, the examples discussed are the axially moving string with clamped ends and rotating circular disk with clamp rim and thus the rigid body motion is not considered. Also the sensors assumed in their derivation are the position and velocity sensors.

In this paper, it is of interest to investigate the controllability and observability of rigid body motion of a magnetically suspended vibration isolation table top. In the case, the table top will be modelled as a rectangular plate with free edges. Due to the importance of the inertial acceleration feedback in vibration isolation systems, the accelerometer outputs are also included in the derivation of the observability condition. Since the prototype design uses magnetic bearings for levitation and vibration control, the unstable nature of the actuators is coupled to the overall

system dynamics. The controllability and observability analysis presented in this work takes this fact into account. In order to apply the results to the system design, normalized frequencies and a map depicting the node lines corresponding to table top were approximated using the Rayleigh-Ritz method.

Improper placement of actuators and sensors can lead to complex control system designs even though these locations may correspond to a controllable and observable system. For example, a conventional flexible arm has zeros in the right half plane if the actuator and sensor are noncollated. This nonminimum phase nature adds additional phase lag to the system and results in poor system performance [8]. Such issues have motivated us to investigate the relationship between proper actuator/sensor locations and favorable open loop system behavior.

In this paper, the problem formulation is presented in section 2. The selection of proper actuator and sensor locations leading to a controllable and observable system is then discussed in section 3. A lumped-parameter model of a flexible vibration isolation table top is used to investigate the system's controllability and observability including the coupling effects introduced by the magnetic bearing. This analysis results in necessary and sufficient conditions for proper selection of actuator and sensor locations. Section 4 presents a favorable pole-zero plot of the open loop transfer functions. Necessary and sufficient conditions for reducing the controller complexity are derived. The results are illustrated by examples using approximate mode shape functions. Such information is important for the overall design of ultra high performance vibration isolation systems. For example, critical frequency regions in the transmissibility curves can be identified and taken into account in the control system design.

2 Problem Formulation

Consider a thin rectangular table top plate with free edges as shown in Figure 1, assuming that the plate is made of homogeneous, isotropic material, then the equation of motion is [9],

$$\rho h \ddot{w}(x,y,t) + D \bigtriangledown^4 w(x,y,t) = f(x,y,t) \tag{1}$$

where ρ is the density of the plate, h is the plate thickness, $w(x,y,t)$ is the transverse deflection, D is the flexural rigidity of the plate and is equal to $\frac{Eh^3}{12(1-\nu^2)}$, E is the Young's modulus, ν is Poisson's ratio and $\bigtriangledown^4$ represents the biharmonic operator . Moreover, since we will first deal with the controllability and observability issues in this paper, only the control force is taken into account and other forces such as gravity and disturbances are not included. Therefore, in such a case $f(x,y,t)$ denotes the control force per unit area of the plate. Because there is no lateral constraint, the boundary conditions of the plate are given by [10],

$$\begin{aligned}
&(i) && \tfrac{\partial^2}{\partial y^2} w(x,y,t) + \nu \tfrac{\partial^2}{\partial x^2} w(x,y,t) = 0 \,|_{0\le x\le a} && \text{for } y=0, y=b \\
&(ii) && \tfrac{\partial^3}{\partial y^3} w(x,y,t) + (2-\nu) \tfrac{\partial^3}{\partial y \partial x^2} w(x,y,t) = 0 \,|_{0\le x\le a} && \text{for } y=0, y=b \\
&(iii) && \tfrac{\partial^2}{\partial x^2} w(x,y,t) + \nu \tfrac{\partial^2}{\partial y^2} w(x,y,t) = 0 \,|_{0\le y\le b} && \text{for } x=0, x=a \\
&(iv) && \tfrac{\partial^3}{\partial x^3} w(x,y,t) + (2-\nu) \tfrac{\partial^3}{\partial x \partial y^2} w(x,y,t) = 0 \,|_{0\le y\le b} && \text{for } x=0, x=a
\end{aligned} \tag{2}$$

The physical meaning of these four boundary conditions is that the bending moments, twist moments, and shear forces along the four edges are equal to zero.

In order to develop and implement a finite dimensional controller, a lumped parameter model of the system is needed for the distributed system described by Equation (1). Because the equation is a partial differential equation, in order to apply the control law, the system should be discretized to obtain a lumped-parameter model. To achieve this we consider only n modes in the dynamic equations and assume that the influence of the higher modes is negligible. The transverse deflection

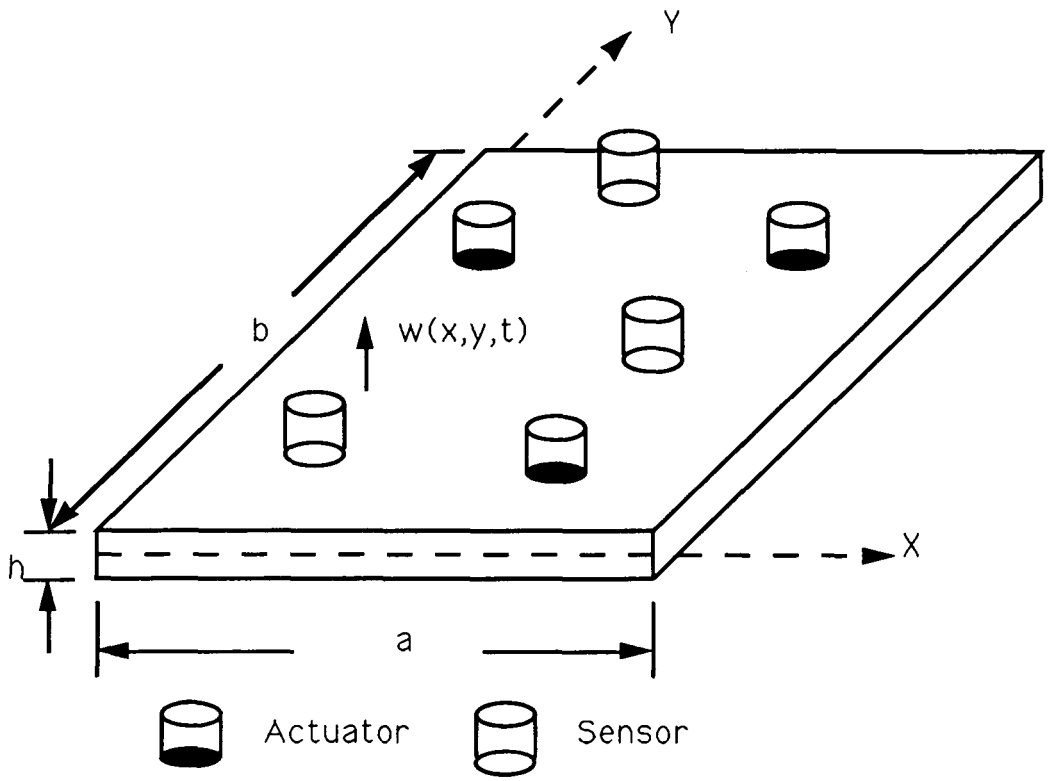

Figure 1: Thin rectangular plate with free edges

$w(x,y,t)$ can be represented by means of a series of n mode shape functions $\phi_i(x,y)$ of the system and expressed in the following form,

$$w(x,y,t) = \sum_{i=1}^{n} a_i(t)\phi_i(x,y) = \mathbf{a}^T(t)\mathbf{\Phi}(x,y) \tag{3}$$

where $a_i(t)$ $(i = 1,2,....,n)$ are the generalized coordinates. We further assume that the table is supported by m discrete point force actuators located at (x_i, y_i) and $i = 1,2,\ldots,m$. Therefore the control force can be expressed as,

$$f(x,y,t) = \sum_{i=1}^{m} f_i(t)\delta_i(x,y) = \mathbf{f}^T(t)\mathbf{\Delta}(x,y) \tag{4}$$

where $f_i(t)$ is the control force exerted by the ith actuator and $\delta_i(x,y)$ is the impulse function at (x_i, y_i). Using Equation (3), the kinetic energy $\mathcal{T}$ and potential energy $\mathcal{V}$ of the plate can be written in terms of generalized coordinates and mode shape functions as [9],

$$\begin{array}{ll} \mathcal{T} = \frac{1}{2}\int_A \rho h\dot{w}^2(x,y,t)dA & = \frac{1}{2}\int_A \rho h[\sum_{i=1}^{n}\dot{a}_i(t)\phi_i(x,y)]^2 dA \\ = \frac{1}{2}\int_A \rho h(\dot{\mathbf{a}}^T\mathbf{\Phi}(x,y))^2 dA & = \frac{1}{2}\dot{\mathbf{a}}^T(t)\mathbf{M}\dot{\mathbf{a}}(t) \end{array} \tag{5}$$

where the inertia matrix $\mathbf{M}$ is given by,

$$\mathbf{M} = \rho h \int_A \mathbf{\Phi}(x,y)\mathbf{\Phi}^T(x,y)dA$$

and

$$\mathcal{V} = \frac{D}{2}\int_A [w_{xx}^2 + w_{yy}^2 + 2\nu w_{xx}w_{yy} + 2(1-\nu)(w_{xy})^2]dA$$

$$
\begin{aligned}
&= \frac{D}{2}\int_A [(\mathbf{a}^T(t)\mathbf{\Phi}_{xx})^2 + (\mathbf{a}^T(t)\mathbf{\Phi}_{yy})^2 + 2\nu\mathbf{a}^T(t)\mathbf{\Phi}_{xx}\mathbf{\Phi}_{yy}^T\mathbf{a}(t) \\
&\quad +2(1-\nu)(\mathbf{a}^T(t)\mathbf{\Phi}_{xy})^2]dA \\
&= \frac{1}{2}\mathbf{a}^T(t)\mathbf{K}\mathbf{a}(t) \qquad (6)
\end{aligned}
$$

where the stiffness matrix $\mathbf{K}$ is given by ,

$$
\begin{aligned}
\mathbf{K} &= D\int_A (\mathbf{\Phi}_{xx}\mathbf{\Phi}_{xx}^T + \mathbf{\Phi}_{yy}\mathbf{\Phi}_{yy}^T \\
&\quad +2\nu\mathbf{\Phi}_{xx}\mathbf{\Phi}_{yy}^T + 2(1-\nu)\mathbf{\Phi}_{xy}\mathbf{\Phi}_{xy}^T)dA
\end{aligned}
$$

Also the virtual work due to the m point force actuators is:

$$
\begin{aligned}
\delta W &= \int_A f(x,y,t)\delta w(x,y,t)dA \\
&= \int_A \mathbf{f}^T(t)\mathbf{\Delta}(x,y)\mathbf{\Phi}^T(x,y)\delta\mathbf{a}(t)dA \\
&= \mathbf{f}^T(t)\left[\int_A \mathbf{\Delta}(x,y)\mathbf{\Phi}^T(x,y)dA\right]\delta\mathbf{a}(t) \\
&= \mathbf{f}^T(t)\mathbf{R}\delta\mathbf{a}(t) \qquad (7)
\end{aligned}
$$

where

$$
\mathbf{R} = \begin{bmatrix} \phi_1^1 & \phi_2^1 & \dots & \phi_n^1 \\ \phi_1^2 & \phi_2^2 & \dots & \phi_n^2 \\ \vdots & \vdots & \dots & \vdots \\ \phi_1^m & \phi_2^m & \dots & \phi_n^m \end{bmatrix}
$$

and ϕ_i^j indicates that the ith mode shape is evaluated at location (x_j, y_j), that is $\phi_i(x_j, y_j)$. Substituting Equations (5), (6), (7) into the variation indicator of the system and applying Hamilton principle, the equations of motion are obtained as,

$$
\mathbf{M}\ddot{\mathbf{a}}(t) + \mathbf{K}\mathbf{a}(t) = \mathbf{R}^T\mathbf{f}(t) \qquad (8)
$$

To transform Equation (8) into a state space form, a state vector $\mathbf{x}^T = [\mathbf{a}^T(t) \quad \dot{\mathbf{a}}^T(t)]$ is introduced so that Equation (8) can be written as,

$$
\dot{\mathbf{x}} = \mathbf{A}\mathbf{x} + \mathbf{B}\mathbf{f} \qquad (9)
$$

where the matrices $\mathbf{A}$ and $\mathbf{B}$ of orders $2n \times 2n$ and $2n \times m$ respectively are given by,

$$
\mathbf{A} = \begin{bmatrix} \mathbf{0} & \mathbf{I} \\ -\mathbf{M}^{-1}\mathbf{K} & \mathbf{0} \end{bmatrix}, \quad \mathbf{B} = \begin{bmatrix} \mathbf{0} \\ \mathbf{M}^{-1}\mathbf{R}^T \end{bmatrix} \qquad (10)
$$

Now that the system equations are formulated, we turn to the system outputs. We consider k sensors located at (x_i, y_i)[1] $(i = 1, 2, ..., s)$. Assuming that the first p sensors are position sensors, $(p+1)th$ to $(p+q)th$ sensors can measure the velocity of the individual points, and the last $s-p-q$ sensors are accelerometers. The outputs from the position sensors can be written as:

$$
y_j(t) = \sum_{i=1}^{n} a_i(t)\phi_i(x_j, y_j) \qquad j = 1, 2, \dots, p \qquad (11)
$$

[1]Even though we use the same notation (x_i, y_i)'s to represent the locations for both actuators and sensors, the point (x_i, y_i) for ith actuator may not be the same as the point (x_i, y_i) for ith sensor.

The outputs from the velocity sensors are :

$$y_j(t) = \sum_{i=1}^{n} \dot{a}_i(t)\phi_i(x_j, y_j) \qquad j = p+1, p+2, \ldots, p+q \tag{12}$$

Finally, the accelerometer outputs are:

$$y_j(t) = \sum_{i=1}^{n} \ddot{a}_i(t)\phi_i(x_j, y_j) \qquad j = p+q+1, p+q+2, \ldots, s \tag{13}$$

Note that $\dot{a}_i(t)$ and $\ddot{a}_i(t)$ represent the first and second time derivatives of the generalized coordinate $a_i(t)$. The overall output equations can now be expressed in matrix form using Equation (11), (12) and (13),

$$\begin{aligned} \mathbf{y} &= \begin{bmatrix} \mathbf{P} & \mathbf{0} \\ \mathbf{0} & \mathbf{Q} \\ \mathbf{0} & \mathbf{0} \end{bmatrix} \mathbf{x}(t) + \begin{bmatrix} \mathbf{0} \\ \mathbf{0} \\ \mathbf{S} \end{bmatrix} \ddot{\mathbf{a}}(t) \\ &= \begin{bmatrix} \mathbf{P} & \mathbf{0} \\ \mathbf{0} & \mathbf{Q} \\ -\mathbf{S}\mathbf{M}^{-1}\mathbf{K} & \mathbf{0} \end{bmatrix} \mathbf{x}(t) + \begin{bmatrix} \mathbf{0} \\ \mathbf{0} \\ \mathbf{M}^{-1}\mathbf{R}^T \end{bmatrix} \mathbf{f}(t) \\ &= \mathbf{C}\mathbf{x} + \mathbf{D}\mathbf{f} \end{aligned} \tag{14}$$

where

$$\mathbf{P}_{p\times n} = \begin{bmatrix} \phi_1^1 & \phi_2^1 & \cdots & \phi_n^1 \\ \phi_1^2 & \phi_2^2 & \cdots & \phi_n^2 \\ \vdots & \vdots & \cdots & \vdots \\ \phi_1^p & \phi_2^p & \cdots & \phi_n^p \end{bmatrix}, \qquad \mathbf{Q}_{q\times n} = \begin{bmatrix} \phi_1^{p+1} & \phi_2^{p+1} & \cdots & \phi_n^{p+1} \\ \phi_1^{p+2} & \phi_2^{p+2} & \cdots & \phi_n^{p+2} \\ \vdots & \vdots & \cdots & \vdots \\ \phi_1^{p+q} & \phi_2^{p+q} & \cdots & \phi_n^{p+q} \end{bmatrix}$$

$$\mathbf{S}_{s\times n} = \begin{bmatrix} \phi_1^{p+q+1} & \phi_2^{p+q+1} & \cdots & \phi_n^{p+q+1} \\ \phi_1^{p+q+2} & \phi_2^{p+q+2} & \cdots & \phi_n^{p+q+2} \\ \vdots & \vdots & \cdots & \vdots \\ \phi_1^{s} & \phi_2^{s} & \cdots & \phi_n^{s} \end{bmatrix}$$

Equation (9) and (14) can now be analyzed in order to determine the conditions of controllability and observability. These issues are addressed in the following section.

3 Controllability and Observability

3.1 Analysis without the Coupling Effect of Actuator Dynamics

The $2nth$ order system described by Equations (9) and (14) is controllable if and only if

$$rank(\mathcal{C}) = rank\begin{bmatrix} \mathbf{B} & \mathbf{AB} & \cdots & \mathbf{A}^{2n-1}\mathbf{B} \end{bmatrix} = 2n \tag{15}$$

and the system is observable if and only if

$$rank(\mathcal{O}) = rank\begin{bmatrix} \mathbf{C}^T & \mathbf{A}^T\mathbf{C}^T & \cdots & (\mathbf{A}^T)^{2n-1}\mathbf{C}^T \end{bmatrix} = 2n \tag{16}$$

In order to simplify the problem and deal with diagonal $\mathbf{M}$ and $\mathbf{K}$ matrices, the orthogonality of the eigenfunctions is used [11]. Under this assumption, the $n \times n$ inertia and stiffness matrices take

the form,

$$\mathbf{M} = \begin{bmatrix} M_1 & 0 & \dots & 0 \\ 0 & M_2 & \dots & 0 \\ \vdots & \vdots & \dots & \vdots \\ 0 & 0 & \dots & M_n \end{bmatrix}, \quad \mathbf{K} = \begin{bmatrix} K_1 & 0 & \dots & 0 \\ 0 & K_2 & \dots & 0 \\ \vdots & \vdots & \dots & \vdots \\ 0 & 0 & \dots & K_n \end{bmatrix} \tag{17}$$

where $M_i, K_i \geq 0$. The matrix $\mathbf{M}^{-1}\mathbf{K}$ is also diagonal with diagonal components corresponding to the system eigenvalues,

$$\mathbf{M}^{-1}\mathbf{K} = \begin{bmatrix} \lambda_1 & 0 & \dots & 0 \\ 0 & \lambda_2 & \dots & 0 \\ \vdots & \vdots & \dots & \vdots \\ 0 & 0 & \dots & \lambda_n \end{bmatrix} \tag{18}$$

The eigenvalues λ_1, λ_2, ..., λ_n are equal to the square of natural frequencies of the system. Because a thin plate with free edges is considered, the first three eigenvalues are equal to zero, i.e., $\lambda_1 = \lambda_2 = \lambda_3 = 0$. The modes associated with these eigenvalues correspond to the translation parallel to the z axis and rigid body rotations along x and y axes. In the following discussion, it is assumed that $n > 3$ so that the vibration modes are taken into account and all other eigenvalues λ_4, λ_5, ..., λ_n are positive. In order to investigate the condition for this system to be controllable and observable, the controllability and observability matrices are calculated and discussed as follows.

In our case , the controllability matrix has the form,

$$\mathcal{C} = \begin{bmatrix} \mathbf{0} & \mathbf{H} & \mathbf{0} & \mathbf{JH} & \dots & \mathbf{0} & \mathbf{J}^{n-1}\mathbf{H} \\ \mathbf{H} & \mathbf{0} & \mathbf{JH} & \mathbf{0} & \dots & \mathbf{J}^{n-1}\mathbf{H} & \mathbf{0} \end{bmatrix} \tag{19}$$

where

$$\mathbf{H}_{n\times m} = \mathbf{M}^{-1}\mathbf{R}^T = \begin{bmatrix} \frac{1}{M_1}\phi_1^1 & \frac{1}{M_1}\phi_1^2 & \dots & \frac{1}{M_1}\phi_1^m \\ \frac{1}{M_2}\phi_2^1 & \frac{1}{M_2}\phi_2^2 & \dots & \frac{1}{M_2}\phi_2^m \\ \vdots & \vdots & \dots & \vdots \\ \frac{1}{M_n}\phi_n^1 & \frac{1}{M_n}\phi_n^2 & \dots & \frac{1}{M_n}\phi_n^m \end{bmatrix}$$

$$\mathbf{J}_{n\times n} = -\mathbf{M}^{-1}\mathbf{K} = \begin{bmatrix} 0 & 0 & 0 & 0 & 0 & \dots & 0 \\ 0 & 0 & 0 & 0 & 0 & \dots & 0 \\ 0 & 0 & 0 & 0 & 0 & \dots & 0 \\ 0 & 0 & 0 & -\lambda_4 & 0 & \dots & 0 \\ 0 & 0 & 0 & 0 & -\lambda_5 & \dots & 0 \\ \vdots & \vdots & \vdots & \vdots & \vdots & \dots & \vdots \\ 0 & 0 & 0 & 0 & 0 & \dots & -\lambda_n \end{bmatrix}$$

Since there are $2n$ states (n position components and n velocity components), the controllability matrix should have rank $2n$ which means that $2n$ rows must be linearly independent. It is obvious that the upper $n \times 2mn$ matrix and the lower $n \times 2mn$ matrix are almost the same except that they are shifted by a series of $n \times m$ $\mathbf{0}$ matrices. Therefore , if n linearly independent rows can be obtained from the upper $n \times mn$ submatrix, the lower $n \times mn$ matrix will also have n linearly independent rows and these two sets of n linearly independent rows are linearly independent to each other. If we interchange the columns of the upper submatrix and put all the 0 columns to the right hand side without changing the rank of the submatrix, we can deduce that the system is controllable if and only if the $n \times mn$ matrix $\mathbf{L}$ has rank n, where

$$\mathbf{L} = \begin{bmatrix} \mathbf{H} & \mathbf{JH} & \dots & \mathbf{J}^{n-1}\mathbf{H} \end{bmatrix} \tag{20}$$

Therefore, the system is controllable if and only if $rank(\mathbf{L}) = n$. Due to the diagonal structure of $\mathbf{J}$ matrix, the conditions for the $\mathbf{L}$ matrix to have rank n are [12]:

1. For λ_i with no repeated eigenvalues, the ith row of the $\mathbf{H}$ matrix should be a nonzero vector.
2. For repeated eigenvalues of multiplicity ℓ, $\lambda_{i+1} = \lambda_{i+2} = \ldots = \lambda_{i+\ell}$, the $(i+1)$th, $(i+2)$th, $\ldots$, $(i+\ell)$th rows of $\mathbf{H}$ should be linearly independent.

On the other hand, the observability matrix takes the form,

$$\mathcal{O} = \begin{bmatrix} \mathbf{P}^T & \mathbf{0} & \mathbf{J}\mathbf{S}^T & \mathbf{0} & \mathbf{J}\mathbf{Q}^T & \mathbf{0} & \ldots & \mathbf{0} & \mathbf{J}^n\mathbf{Q}^T & \mathbf{0} \\ \mathbf{0} & \mathbf{Q}^T & \mathbf{0} & \mathbf{P}^T & \mathbf{0} & \mathbf{J}\mathbf{S}^T & \ldots & \mathbf{J}^{n-1}\mathbf{P}^T & \mathbf{0} & \mathbf{J}^n\mathbf{S}^T \end{bmatrix} \tag{21}$$

To investigate the rank of this matrix , we rearrange it as follows:

$$\mathcal{O}' = \begin{bmatrix} \mathbf{P}^T & \mathbf{J}\mathbf{S}^T & \mathbf{J}\mathbf{Q}^T & \ldots & \mathbf{J}^n\mathbf{Q}^T & \mathbf{0} & \mathbf{0} & \mathbf{0} & \ldots & \mathbf{0} \\ \mathbf{0} & \mathbf{0} & \mathbf{0} & \ldots & \mathbf{0} & \mathbf{P}^T & \mathbf{Q}^T & \mathbf{J}\mathbf{S}^T & \ldots & \mathbf{J}^n\mathbf{S}^T \end{bmatrix} \tag{22}$$

For the system to be observable, the following two conditions must be satisfied,

$$rank\begin{bmatrix} \mathbf{P}^T & \mathbf{J}\mathbf{S}^T & \mathbf{J}\mathbf{Q}^T & \ldots & \mathbf{J}^n\mathbf{Q}^T \end{bmatrix} = rank\begin{bmatrix} \mathbf{H}' & \mathbf{J}\mathbf{H}' & \ldots & \mathbf{J}^{n-1}\mathbf{H}' \end{bmatrix} = n \tag{23}$$

where $\mathbf{H}' = [\mathbf{P}^T \;\; \mathbf{J}\mathbf{S}^T \;\; \mathbf{J}\mathbf{Q}^T]$, and

$$rank\begin{bmatrix} \mathbf{P}^T & \mathbf{Q}^T & \mathbf{J}\mathbf{S}^T & \ldots & \mathbf{J}^n\mathbf{S}^T \end{bmatrix} = rank\begin{bmatrix} \mathbf{H}'' & \mathbf{J}\mathbf{H}'' & \ldots & \mathbf{J}^{n-1}\mathbf{H}'' \end{bmatrix} = n \tag{24}$$

where $\mathbf{H}'' = [\mathbf{P}^T \;\; \mathbf{Q}^T \;\; \mathbf{J}\mathbf{S}^T]$. By substituting the $\mathbf{P}$, $\mathbf{Q}$, and $\mathbf{S}$ matrices, the $\mathbf{H}'$, $\mathbf{H}''$ matrices in Equation (23) and (24) can be represented as,

$$\mathbf{H}' = \begin{bmatrix} \phi_1^1 & \ldots & \phi_1^p & 0 & \ldots & 0 & 0 & \ldots & 0 \\ \phi_2^1 & \ldots & \phi_2^p & 0 & \ldots & 0 & 0 & \ldots & 0 \\ \phi_3^1 & \ldots & \phi_3^p & 0 & \ldots & 0 & 0 & \ldots & 0 \\ \phi_4^1 & \ldots & \phi_4^p & (-\lambda_4)\phi_4^{p+1} & \ldots & (-\lambda_4)\phi_4^{p+q} & (-\lambda_4)\phi_4^{p+q+1} & \ldots & (-\lambda_4)\phi_4^s \\ \vdots & \ldots & \vdots & \vdots & \ldots & \vdots & \vdots & \ldots & \vdots \\ \phi_n^1 & \ldots & \phi_n^p & (-\lambda_n)\phi_n^{p+1} & \ldots & (-\lambda_n)\phi_n^{p+q} & (-\lambda_n)\phi_n^{p+q+1} & \ldots & (-\lambda_n)\phi_n^s \end{bmatrix} \tag{25}$$

and

$$\mathbf{H}'' = \begin{bmatrix} \phi_1^1 & \ldots & \phi_1^p & \phi_1^{p+1} & \ldots & \phi_1^{p+q} & 0 & \ldots & 0 \\ \phi_2^1 & \ldots & \phi_2^p & \phi_2^{p+1} & \ldots & \phi_2^{p+q} & 0 & \ldots & 0 \\ \phi_3^1 & \ldots & \phi_3^p & \phi_3^{p+1} & \ldots & \phi_3^{p+q} & 0 & \ldots & 0 \\ \phi_4^1 & \ldots & \phi_4^p & \phi_4^{p+1} & \ldots & \phi_4^{p+q} & (-\lambda_4)\phi_4^{p+q+1} & \ldots & (-\lambda_4)\phi_4^s \\ \vdots & \ldots & \vdots & \vdots & \ldots & \vdots & \vdots & \ldots & \vdots \\ \phi_n^1 & \ldots & \phi_n^p & \phi_n^{p+1} & \ldots & \phi_n^{p+q} & (-\lambda_n)\phi_n^{p+q+1} & \ldots & (-\lambda_n)\phi_n^s \end{bmatrix} \tag{26}$$

Due to the similarity between the observability Equations (23), (24) and the controllability Equation (20), the system is observable if both $\mathbf{H}'$ and $\mathbf{H}''$ matrices satisfy conditions (1) and (2). Therefore, the relation between the location of actuators (sensors) and controllability (observability) can be obtained. These results are summarized in the following theorems.

Theorem 3.1 *If the kth mode is controllable (observable), then there exists st least one actuator (sensor) not located on the corresponding node loci.*

Proof: In condition (1), the *ith* row vector of $\mathbf{H}$ ($\mathbf{H}'$, $\mathbf{H}''$) should be a nonzero vector. This corresponds to the situation that for every mode shape function $\phi_i(x, y)$ with no repeated eigenvalue, there exists one actuator (sensor) location (x_j, y_j) such that $\phi_i(x_j, y_j) = \phi_i^j$ is nonzero. □

Theorem 3.2 *ℓ modes with the same natural frequency ($\lambda_{i+1} = \lambda_{i+2} = \ldots = \lambda_{i+\ell}$) are controllable (observable) if there exists at least ℓ actuators (sensors) located at points $(x_{j_\alpha}, y_{j_\alpha})$ $(\alpha = 1, 2, ...\ell)$ such that*

$$det \begin{bmatrix} \phi_{i+1}^{j_1} & \phi_{i+1}^{j_2} & \cdots & \phi_{i+1}^{j_\ell} \\ \vdots & \vdots & \cdots & \vdots \\ \phi_{i+\ell}^{j_1} & \phi_{i+\ell}^{j_2} & \cdots & \phi_{i+\ell}^{j_\ell} \end{bmatrix} \neq 0 \tag{27}$$

where $\phi_{i+1}, \phi_{i+2}, \ldots, \phi_{i+\ell}$ are the mode shape functions or the eigenfunctions corresponding to this natural frequency.

Proof: In condition (2), the $(i+1)th$, $(i+2)th$, ..., $(i+\ell)th$ rows of $\mathbf{H}$ ($\mathbf{H}'$, $\mathbf{H}''$) are linearly independent if there are ℓ linearly independent columns in the submatrix formed by the $i+1th$, $i+2th$, ..., $i+\ell th$ rows of $\mathbf{H}$ matrix. This corresponds to the situation for which every set of ℓ mode shape functions ϕ_{i+1}, ..., $\phi_{i+\ell}$ corresponding to same eigenvalue $\lambda_{i+1} = \lambda_{i+2} = \ldots = \lambda_{i+\ell}$, there should exist a set of $(x_{j_\alpha}, y_{j_\alpha})$ $(\alpha = 1, 2, \ldots \ell)$ such that Equation (27) is satisfied. □
A direct application of this result is that there should be at least α actuators (sensors) not located at the intersections of all the node lines of the same natural frequencies to make these modes controllable (observable).

Theorem 3.3 *The modes of a flexible plate cannot be controlled (observed) with less than three actuators (position sensors) , nor is it possible to control (observe) them with more than three collinear actuators (sensors).*

Proof: Since there are three zero eigenvalues corresponding to rigid body motion, it can therefore be concluded that there should exist a set of three actuator (or position sensor, due to the 0 submatrix in the upper-right corners of $\mathbf{H}'$ and $\mathbf{H}''$ matrices) locations (x_{j_1}, y_{j_1}), (x_{j_2}, y_{j_2}), (x_{j_3}, y_{j_3}) so that,

$$det \begin{bmatrix} \phi_1^{j_1} & \phi_1^{j_2} & \phi_1^{j_3} \\ \phi_2^{j_1} & \phi_2^{j_2} & \phi_2^{j_3} \\ \phi_3^{j_1} & \phi_3^{j_2} & \phi_3^{j_3} \end{bmatrix} \neq 0 \quad \text{for some } j_1, j_2, j_3 \text{ between 1 and } m\ (p) \tag{28}$$

$\phi_1(x, y)$, $\phi_2(x, y)$ and $\phi_3(x, y)$ denote the first three mode shape functions of the plate which correspond to one parallel translation and two rigid body rotations. Assuming $\phi_1(x, y) = 1$, $\phi_2(x, y) = x$, $\phi_3(x, y) = y$, Equation (28) implies that there exists three actuator (position sensor) locations (x_{j_i}, y_{j_i}) $(i = 1, 2, 3)$ such that,

$$det \begin{bmatrix} 1 & 1 & 1 \\ x_{j_1} & x_{j_2} & x_{j_3} \\ y_{j_1} & y_{j_2} & y_{j_3} \end{bmatrix} \neq 0 \quad \text{for some } j_1, j_2, j_3 \text{ between 1 and } m\ (p) \tag{29}$$

which means that these three points are not collinear. □

Corollary 3.1 *The minimum number of properly located actuators (sensors) necessary to control (observe) the modes of a flexible plate is equal to max { 3, multiplicity of eigenvalue of the modes to control (observe) }.*

Proof: This is the direct result from the previous three theorems. □

3.2 Analysis with the Coupling Effect of Actuator Dynamics

In the previous discussion of controllability and observability, no actuator dynamics were considered in the system state equation. Since we are interested in using magnetically levitation techniques to control the vibration, the unstable nature of magnetic forces should be taken into account. This

instability comes from the negative stiffness existing between the levitated object and the magnetic bearing pole face. The introduction of magnetic bearings into the system will significantly affect the dynamic behavior. Therefore, in this section we reformulate the problem and investigate the influence of magnetic bearings on the controllability and observability conditions. In general, the nonlinear magnetic force equation is linearized about an equilibrium point. The incremental force can then be represented by,

$$f = k_z z + k_i i \tag{30}$$

where k_z is the unstable stiffness, z is the air gap distance, k_i is the current stiffness constant and i is the control current. Assuming m magnetic bearings are used as actuators in the vibration isolation system, then Equation (30) is written in vector form as,

$$\mathbf{f} = \mathcal{K}_z \mathbf{z} + \mathcal{K}_i \mathbf{i} \tag{31}$$

In this equation, $\mathbf{f}, \mathbf{z}, \mathbf{i}$ denote the $m \times 1$ force, air gap distance, and control current vectors. $\mathcal{K}_z$[2] and $\mathcal{K}_i$ are both nonsingular , $m \times m$ diagonal matrices. The diagonal elements of $\mathcal{K}_z$ represent the unstable stiffness of each magnetic bearing while those of $\mathcal{K}_i$ are the corresponding current stiffness constants. Substituting Equation (31) into Equation(9) and using the relation that $\mathbf{z} = [\mathbf{R} \quad \mathbf{0}]\mathbf{x}$, we can get the new state equation as,

$$\dot{\mathbf{x}} = \mathbf{A}'\mathbf{x} + \mathbf{B}'\mathbf{i} \tag{32}$$

where

$$\mathbf{A}' = \begin{bmatrix} \mathbf{0} & \mathbf{I} \\ \mathbf{J} + \mathbf{H}\mathcal{K}_z\mathbf{R} & \mathbf{0} \end{bmatrix}, \quad \mathbf{B}' = \begin{bmatrix} \mathbf{0} \\ \mathbf{H}\mathcal{K}_i \end{bmatrix} \tag{33}$$

Using the same procedure as discussed previously, the system is controllable if and only if the matrix

$$\mathbf{L}' = \Big[\mathbf{H}\mathcal{K}_i \quad (\mathbf{J} + \mathbf{H}\mathcal{K}_z\mathbf{R})\mathbf{H}\mathcal{K}_i \quad (\mathbf{J} + \mathbf{H}\mathcal{K}_z\mathbf{R})^2\mathbf{H}\mathcal{K}_i \quad \ldots \quad (\mathbf{J} + \mathbf{H}\mathcal{K}_z\mathbf{R})^{n-1}\mathbf{H}\mathcal{K}_i\Big] \tag{34}$$

has rank n. A first result is stated in the following lemma.

Lemma 3.1 *Given an integer p and matrices $\mathbf{J}$, $\mathbf{H}$ and $\mathbf{W}$ such that $p \in Z$, $\mathbf{J} \in R^{n\times n}$, $\mathbf{H} \in R^{n\times m}$ and $\mathbf{W} \in R^{m\times m}$, The column space of the matrix $\mathbf{J}^p\mathbf{H}\mathbf{W}$ is spanned by the column vectors of the matrix $\mathbf{J}^p\mathbf{H}$.*

Proof: Assuming that the matrix $\mathbf{H} = [\mathbf{h}_1 \quad \mathbf{h}_2 \quad \ldots \quad \mathbf{h}_m]$ where the $\mathbf{h}_i$'s are column vectors of $\mathbf{H}$. Let the elements of $\mathbf{W}$ be w_{ij}, then

$$\begin{aligned} \mathbf{J}^p\mathbf{H}\mathbf{W} &= \mathbf{J}^p[\mathbf{h}_1 \quad \mathbf{h}_2 \quad \ldots \quad \mathbf{h}_m]\mathbf{W} \\ &= \mathbf{J}^p\left[\sum_{j=1}^{m} w_{j,1}\mathbf{h}_j \quad \sum_{j=1}^{m} w_{j,2}\mathbf{h}_j \quad \ldots \quad \sum_{j=1}^{m} w_{j,n}\mathbf{h}_j\right] \\ &= \left[\sum_{j=1}^{m} w_{j,1}\mathbf{J}^p\mathbf{h}_j \quad \sum_{j=1}^{m} w_{j,2}\mathbf{J}^p\mathbf{h}_j \quad \ldots \quad \sum_{j=1}^{m} w_{j,n}\mathbf{J}^p\mathbf{h}_j\right] \end{aligned}$$

Because $\mathbf{J}^p\mathbf{H}$ can be expanded as $[\mathbf{J}^p\mathbf{h}_1 \quad \mathbf{J}^p\mathbf{h}_2 \quad \ldots \quad \mathbf{J}^p\mathbf{h}_m]$, it is obvious that the column space of $\mathbf{J}^p\mathbf{H}\mathbf{W}$ is spanned by the column vectors of $\mathbf{J}^p\mathbf{H}$. □

Now we state a controllability theorem for magnetically levitated vibration isolation system..

[2]Due to the instability of the magnetic bearing, $\mathcal{K}_z$ is a positive definite matrix.

Theorem 3.4 *The system described by Equation (9) is controllable if and only if the system described by Equation (32).*

Proof: In order to show this, we need to prove that the rank of $\mathbf{L}'$ is the same as that of $\mathbf{L}$. Since $\mathcal{K}_i$ is a common factor in each element of $\mathbf{L}'$, we can factor it out and write the $\mathbf{L}'$ matrix as,

$$\mathbf{L}' = \mathbf{L}''\mathcal{K}_i$$

where $\mathbf{L}'' = \left[\mathbf{H} \quad (\mathbf{J}+\mathbf{H}\mathcal{K}_z\mathbf{R})\mathbf{H} \quad (\mathbf{J}+\mathbf{H}\mathcal{K}_z\mathbf{R})^2\mathbf{H} \quad \ldots \quad (\mathbf{J}+\mathbf{H}\mathcal{K}_z\mathbf{R})^{n-1}\mathbf{H}\right]$. Since $\mathcal{K}_i$ is a nonsingular diagonal matrix, $\mathbf{L}''$ has the same rank as the matrix $\mathbf{L}'$. We perform the algebraic manipulation on column vectors to reduce the $\mathbf{L}''$ matrix into the same form as the $\mathbf{L}$ matrix. From the lemma for the case of $p = 0$, we can use the columns of $\mathbf{H}$, which is the first element of $\mathbf{L}''$ to eliminate $\mathbf{H}\mathcal{K}_z\mathbf{R}\mathbf{H}$ in the second element so that only the columns of $\mathbf{JH}$ remains. Then expand the third element as $\mathbf{J}^2\mathbf{H} + \mathbf{JH}\mathcal{K}_z\mathbf{RH} + \mathbf{H}\mathcal{K}_z\mathbf{RJH} + \mathbf{H}\mathcal{K}_z\mathbf{RH}\mathcal{K}_z\mathbf{RH}$. The lemma again allows us to use the the columns of first element $\mathbf{H}$ and the new second element $\mathbf{JH}$ to reduce the third element into $\mathbf{J}^2\mathbf{H}$. Applying the same column reduced procedure to the $4th, 5th, \ldots, nth$ elements of $\mathbf{L}''$ matrix. We can reduced the $\mathbf{L}''$ into the same matrix as $\mathbf{L}$. The algebraic manipulation of column vectors doesn't change the rank of the matrix $\mathbf{L}''$, therefore we conclude that the $\mathbf{L}''$ matrix and the $\mathbf{L}$ matrix have the same rank, which implies $\mathbf{L}'$ matrix has the same rank as $\mathbf{L}$. □

A direct application of the theorem is that the introduction of the magnetic bearings dynamics wouldn't influence the controllability condition discussed previously. And all the theorems mentioned before can be applied to the magnetic levitated vibration isolation systems.

For the observability part, using the same argument, we can prove the magnetic bearing dynamics wouldn't change the observability condition if there are m position sensors collocated with those m magnetic bearings. This is because if the m position sensors collocated with those m magnetic bearings used, the $m \times 1$ output vector becomes $\mathbf{y} = [\mathbf{R} \quad \mathbf{0}]\mathbf{x}$. Using Equation (32), the observability condition can be deduced and is in fact similar to the controllability condition of Equation (34).

3.3 Examples of Locating Actuators (Sensors) to Achieve Controllability (Observability)

To apply the results obtained in the previous section, the eigenfunctions or the mode shape functions of the system need to be determined. Since there is no analytical solution for a flexible plate with free edges [13], approximate mode shape functions are found using with the Rayleigh-Ritz method. These mode shape functions allow us to get the node loci, which are the locus of points on the plate with zero amplitude corresponding to the normalized natural frequency. For the case of a square plate, the node loci of different normalized natural frequencies are shown in Figure 2. From the relationships obtained from the previous section, to control and observe the vibration of the plate, it can be inferred that we have to choose the actuators and sensors not located on the node loci associated with the desired frequency. Therefore, Figure 2 can be used as a guide line to properly locate the actuators and sensors so that the modes of interest may be controlled (observed) efficiently. Of course, it is necessary to check whether these locations satisfy the condition of linear independence for the modes with the same natural frequency.

In order to apply the results obtained from the discussion of controllability and observability, the first 9 node loci together as a node map are shown in Figure 3. Some examples of locating the actuators and sensors are illustrated as follows:

In Figure 4, the three actuators (sensors) are located in a straight line. Therefore, the rigid body rotation of the plate about this line cannot be controlled (observed).

As shown in Figure 5, although the three actuators (sensors)aren't collinear, they are all placed on the node line of the sixth mode. Therefore, this mode cannot be controlled (observed).

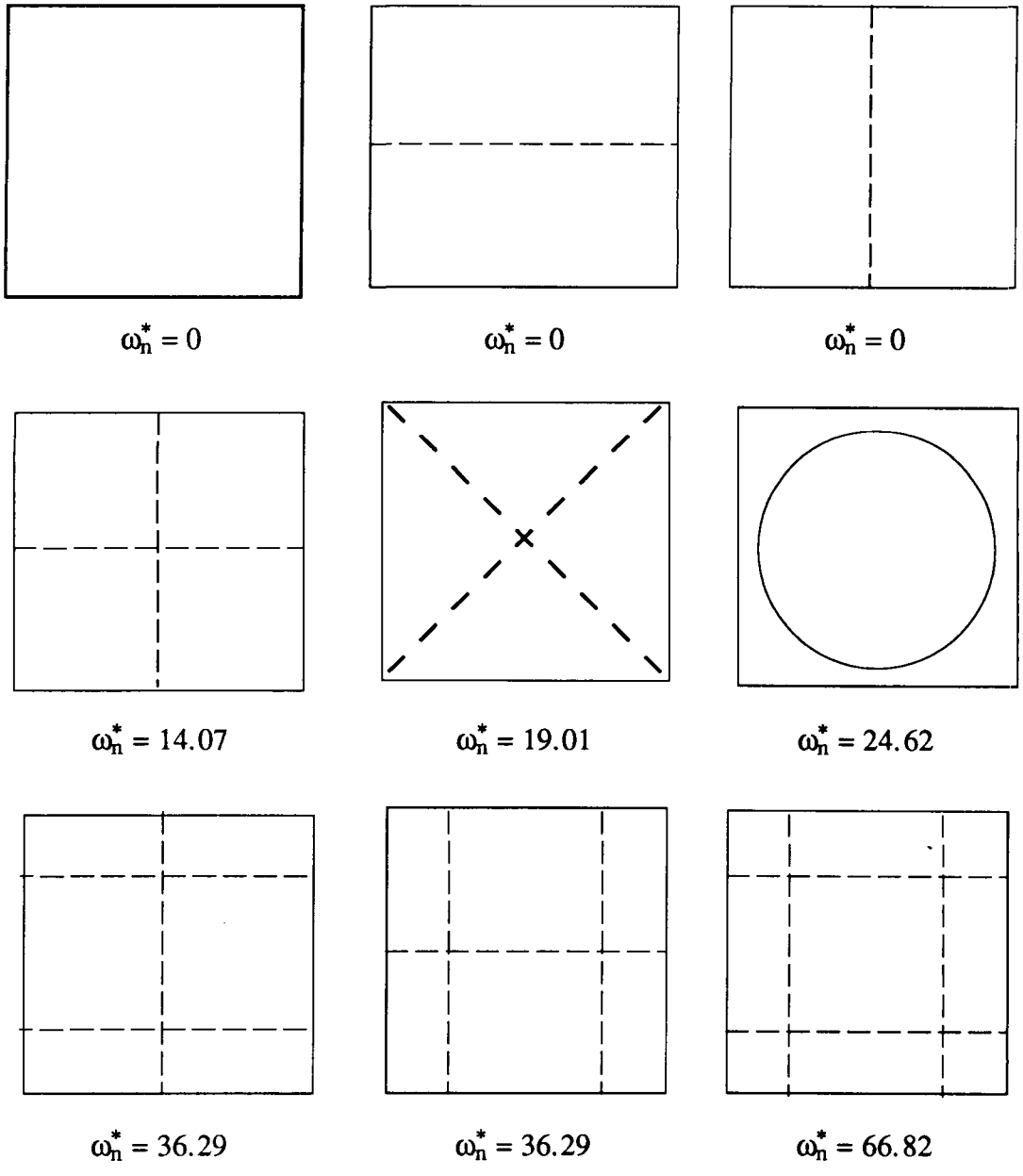

Figure 2: The node loci of the first nine normalized frequencies

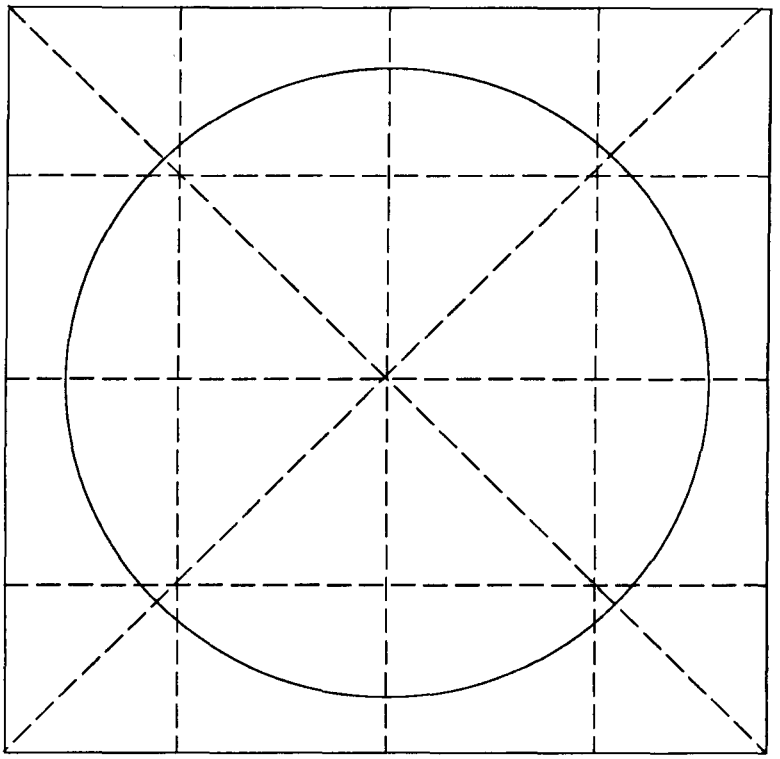

Figure 3: Node map of the first 9 modes of vibration

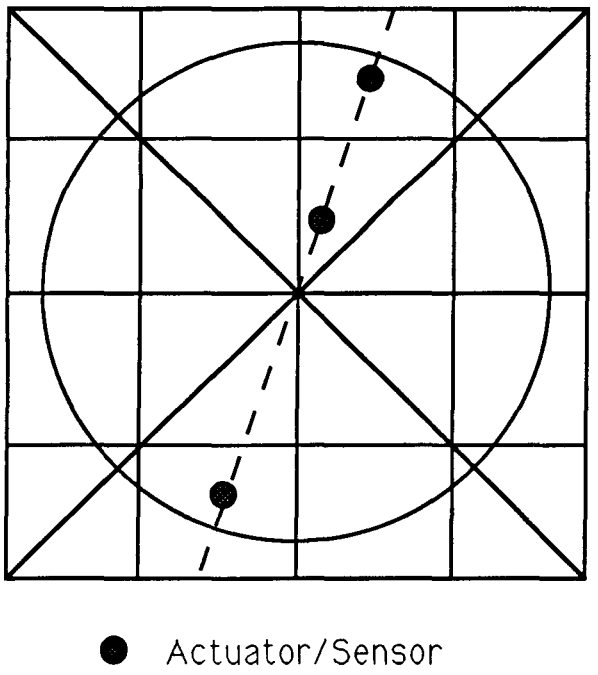

Figure 4: Uncontrollability (unobservability) due to three collinear actuators (sensors)

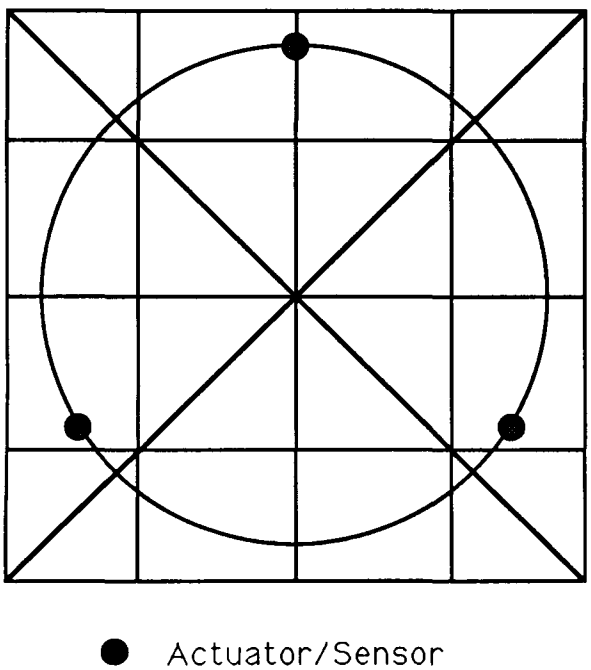

Figure 5: Uncontrollability (unobservability) of the sixth mode due to actuators (sensors) located on the node line of this mode

In Figure 6, since one actuator (sensor) is not located on any node line of the nine modes, it seems that all the nine modes are controllable (observable). However, due to the fact that the other two actuators and/or sensors are located at the intersections of the node line corresponding to the normalized frequency $\omega^* = 36.29$, the condition for repeated eigenvalues makes these two modes uncontrollable (unobservable).

Figure 7 shows four actuators (sensors) placed in symmetrical arrangement on the node line of the fourth mode. Therefore, the fourth mode is uncontrollable (unobservable).

Figure 8 shows three actuators (sensors) which are located unsymmetrically on the plate. All of the nine modes in this are controllable (observable) because none of the actuators (sensors) are located on the node lines.

4 Control System Characteristics for Collocated and Non-collocated Configurations

In this section, we will examine proper actuator/sensor locations leading to a favorable open-loop system behavior. We will investigate the influence of the collocated and noncollocated actuator/sensor configuration on the control system characteristics, and then provide guide lines for achieving a favorable system behavior.

The open loop transfer function matrix of the $2nth$ order system described by Equations (9) and (14) is,

$$\mathbf{G}(s) = \mathbf{C}(s\mathbf{I} - \mathbf{A})^{-1}\mathbf{B} \tag{35}$$

In the following analysis, it is assumed that only position sensors are used which corresponds to that $\mathbf{C} = [\mathbf{P} \quad 0]$. If the corresponding elements of matrices $\mathbf{A}, \mathbf{B}$ and $\mathbf{C}$ are substituted into the

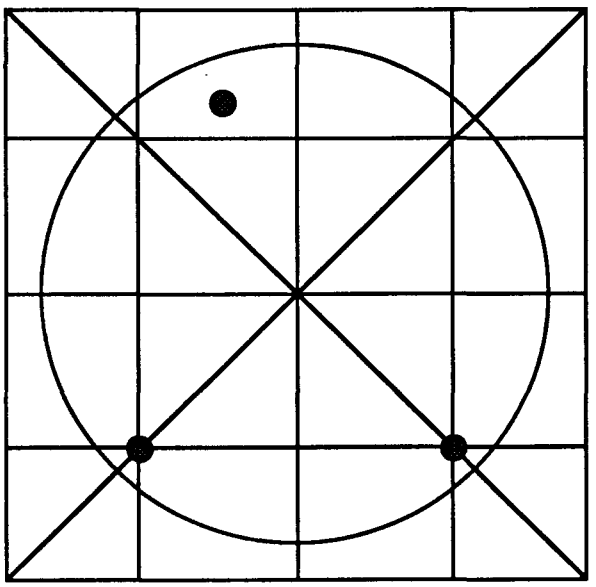

● Actuator/Sensor

Figure 6: Uncontrollability (unobservability) of the seventh and eighth modes

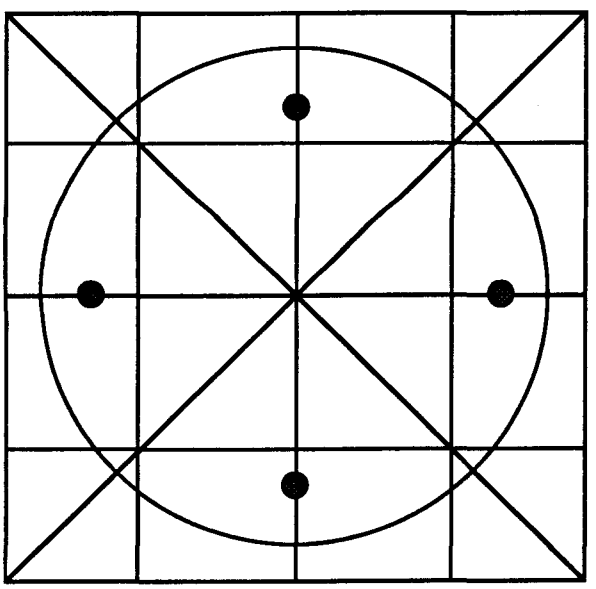

● Actuator/Sensor

Figure 7: Uncontrollability (unobservability) of the fourth modes

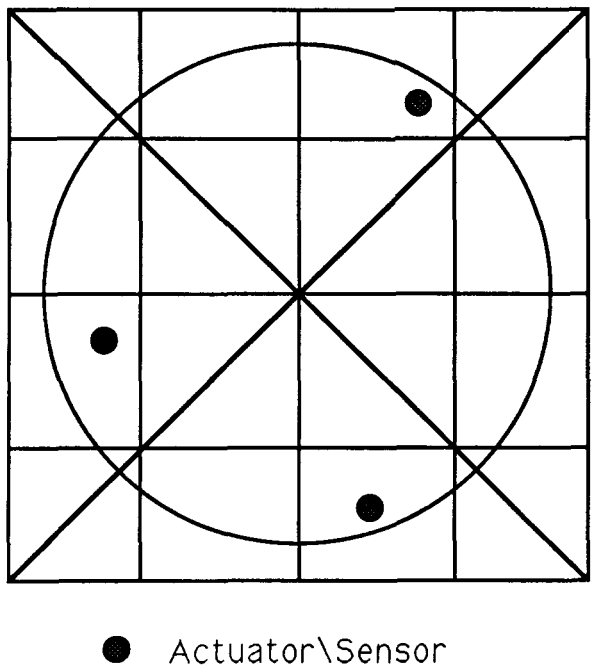

Figure 8: Controllability (observability) using three actuators (sensors)

right hand side of Equation (35), then the $(i,j)th$ element of the $\mathbf{G}(s)$ matrix takes the form,

$$\begin{aligned} g_{i,j}(s) &= \sum_{k=1}^{n} \frac{\phi_k^{s_i}\phi_k^{a_j}}{M_k(s^2+\omega_k^2)} \\ &= \frac{\sum_{k=1}^{n}\left[\frac{\phi_k^{s_i}\phi_k^{a_j}}{M_k}\prod_{\ell=1,\ell\neq k}^{n}(s^2+\omega_\ell^2)\right]}{\prod_{k=1}^{n}(s^2+\omega_k^2)} \end{aligned} \tag{36}$$

$g_{i,j}(s)$ denotes the transfer function from the jth actuator at location (x_{a_j}, y_{a_j}) to the ith sensor at location (x_{s_i}, y_{s_i}).

The transfer function $g_{i,j}(s)$, if without pole-zero cancellation, always has poles at $\pm\mathbf{j}\omega_1$, $\pm\mathbf{j}\omega_2$, ..., $\pm\mathbf{j}\omega_n$. If with pole-zero cancellation is possible, we can skip those cancellation pairs and focus only on the uncancelled ones. The numerator of Equation (36) has to be expanded as an $2(n-1)th$ degree polynomial and solved for the $2(n-1)$ zeros. Because the coefficients of this polynomial are real and the Laplace variable s always appear with even power, if there is any complex root $\alpha+\mathbf{j}\beta$, then $\alpha-\mathbf{j}\beta$, $-\alpha+\mathbf{j}\beta$ and $-\alpha+\mathbf{j}\beta$ are also the roots of the polynomial. Therefore, for the transfer function to be nonminimum phase, the zeros can't be any positive or complex numbers. This implies that the zeros, like the poles, should be on the imaginary axis. Although such information may be known, there are still many ways to locate the zeros. In order to decide on the most favorable type of pole-zero plot, the merits of a conventional PD controller are evaluated. The following lemma and theorem allow us to compare the relative performances of different types of pole-zero plots.

Lemma 4.1 *For a system with the transfer function in the form of Equation (36), if the ith pole located at $\pm\mathbf{j}\omega_i$ is stabilized by a PD controller and there are $2\ell_i$ zeros at $\pm\mathbf{j}\beta_1$, $\pm\mathbf{j}\beta_2$, ..., $\pm\mathbf{j}\beta_{\ell_i}$ such that $\beta_1 < \beta_2 < \ldots < \beta_{\ell_i} < \omega_i$, then $\ell_i - i = 2q_i - 1$ where q_i is an arbitrary integer.*

Proof: To prove this lemma, we look at the angle of departure of the ith pole. The angle of departure α_i of the ith pole is equal to 180^o−(sum of the angles of vectors to this poles from other

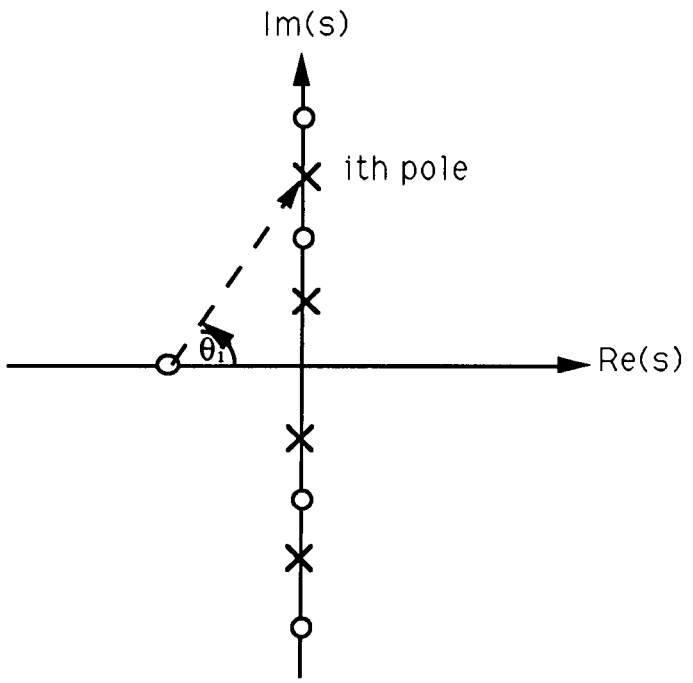

Figure 9: Calculation of the angle of departure for a PD controller

poles)+(sum of the angles of vectors to this pole from zeros) [14]. For the pole-zero plot shown in Figure (9), it can be shown that,

$$\begin{aligned} \alpha_i &= 180^o - [(n+i-1)\times 90^o - (n-i)\times 90^o] + [\theta_i + (n-1+\ell)\times 90^o - (n-1-\ell)\times 90^o] \\ &= 180^o + \theta_i + (2\ell - 2i + 1)\times 90^o \end{aligned} \tag{37}$$

Because a stable PD controller is used, $0 < \theta < 90^o$, which means $180^o + (2\ell - 2i + 1)\times 90^o < \alpha_i < 270^o + (2\ell - 2i + 1)\times 90^o$. It is obvious that if the root locus of the *ith* pole goes to the stable region, then $90^o \leq \alpha_i \leq 270^o$. Equation (37) can satisfy this angle condition only when $2\ell + 2i + 1 = 4q_i - 1$, that is , $\ell_i - i = 2q_i - 1$. □

Theorem 4.1 *If all* $2n$ *poles* $\pm j\omega_1$, $\pm j\omega_2$, ..., $\pm j\omega_n$ *in Equation (36) are stabilized by a PD controller, then there should be one and only zero located between two consecutive poles* $j\omega_i$, $j\omega_{i+1}$ *or* $-j\omega_i$, $-j\omega_{i+1}$ *for* $i = 1, 2, \ldots, n-1$. *And the pole-zero plot should be the same as the one shown in Figure (10).*

Proof: For all the poles to be stablized by a PD controller, Lemma 4.1 should be true for all poles. Take the poles located at $j\omega_i$, $j\omega_{i+1}$ or $-j\omega_i$, $-j\omega_{i+1}$ for example, the necessary condition becomes,

$$\begin{aligned} \ell_{i+1} - (i+1) &= 2q_{i+1} - 1 \qquad (a) \\ \ell_i - i &= 2q_i - 1 \qquad (b) \end{aligned}$$

If (b) is substracted from (a), we get $\ell_{i+1} - \ell_i = 2(q_{i+1} - q_i) + 1$ which implies that $\ell_{i+1} - \ell_i$ is an odd number. Since $\ell_{i+1} - \ell_i$ represents the number of zeros between these two poles and can't be a negative number. From above arguments, $\ell_{i+1} - \ell_i$ has to be greater than or equal to 1. This means that there is at least one zero between two poles $j\omega_i$, $j\omega_{i+1}$ or $-j\omega_i$, $-j\omega_{i+1}$. Because there is only $2(n-1)$ zeros for this transfer function and we have to place at least one zero in each of

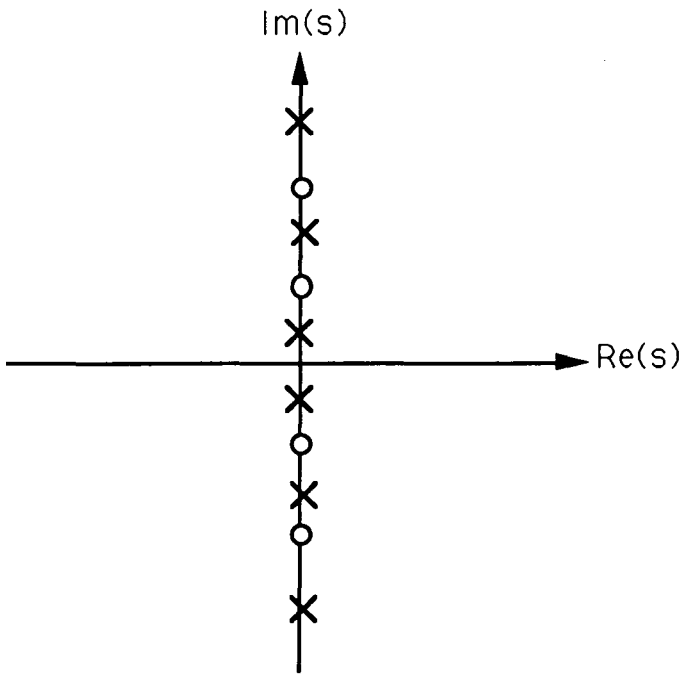

Figure 10: A favorable pole-zero plot

the $2(n-1)$ intervals between consecutive poles $\mathbf{j}\omega_i$, $\mathbf{j}\omega_{i+1}$ or $-\mathbf{j}\omega_i$, $-\mathbf{j}\omega_{i+1}$ for $i = 1, 2, \ldots, n$, the only pole-zero type can be achieved is the alternating pole-zero plot shown in Figure (10). □

Now we have proved that the only type of nonminimum phase pole-zero plot can be stabilized by a conventional PD controller is the alternating pole-zero plot. In what follows, we limit ourselves to this case and investigate the condition on the transfer function to have such a dynamic behavior. This condition can be obtained from the following theorem,

Theorem 4.2 *The transfer function of Equation (36) has an alternating pole-zero plot as in Figure (10) if and only if either one of the following conditions is true,*

(i)	$\frac{\phi_k^{s_i}\phi_k^{a_j}}{M_k}$	$>$	0	*for any kth mode with no repeated eigenvalues*
and	$\sum_{k=p+1}^{p+q}[\frac{\phi_k^{s_i}\phi_k^{a_j}}{M_k}]$	$>$	0	*for p+1th, p+2th, ..., p+qth modes with same repeated eigenvalues*
or				
(ii)	$\frac{\phi_k^{s_i}\phi_k^{a_j}}{M_k}$	$<$	0	*for any kth mode with no repeated eigenvalues*
and	$\sum_{k=p+1}^{p+q}[\frac{\phi_k^{s_i}\phi_k^{a_j}}{M_k}]$	$<$	0	*for p+1th, p+2th, ..., p+qth modes with same repeated eigenvalues*

Proof: To simplify the notation, a_k's are used to denote $\frac{\phi_k^{s_i}\phi_k^{a_j}}{M_k}$ and all the eigenvalues are different. This condition will be relaxed later. Then the numerator $Z(s)$ of Equation (36) can be written as,

$$Z(s) = \sum_{k=1}^{n} a_k \prod_{\ell=1,\ell\neq k}^{n} (s^2 + \omega_\ell^2) \tag{38}$$

The $2(n-1)$ roots of $Z(s)$ which are represented by $\pm \mathbf{j}z_1$, $\pm \mathbf{j}z_2$, ..., $\pm \mathbf{j}z_{n-1}$ correspond to the zeros of the transfer function. For the system to have alternating pole-zero plot, we should have $\omega_k < z_k < \omega_{k+1}$ for $k = 1, 2, \ldots, n-1$. The necessary and sufficient condition for the above arguments to be true is,

$$Z(\mathbf{j}\omega_k)Z(\mathbf{j}\omega_{k+1}) = a_k a_{k+1} \prod_{\ell=1,\ell\neq k}^{n} (-\omega_k^2 + \omega_\ell^2) \prod_{\ell=1,\ell\neq k+1}^{n} (-\omega_{k+1}^2 + \omega_\ell^2) < 0$$
$$\text{for } k = 1,\ 2,\ \ldots,\ n-1 \tag{39}$$

Since $\omega_1 < \omega_2 < \ldots < \omega_n$, the following product must be negative,

$$\begin{aligned} sgn[\prod_{\ell=1,\ell\neq k}^{n} (-\omega_k^2 + \omega_\ell^2) \prod_{\ell=1,\ell\neq k+1}^{n} (-\omega_{k+1}^2 + \omega_\ell^2)] &= sgn[(-1)^{k-1}(-1)^k] \\ &= -1 \end{aligned} \tag{40}$$

If this result is substitubed into Equation (39), the necessary and sufficient condition becomes $a_k a_{k+1} > 0$ for $k = 1, 2, \ldots, n-1$. This condition is the same as either $a_k > 0$ or $a_k < 0$ for any k, which means that all the a_k's have the same sign. If there are $p+1th$, $p+2th$, ..., $p+qth$ with the same natural frequency, then in Equation (36), all the $p+1th$, $p+2th$, ..., $p+qth$ can be summed up together so that there is no repeated poles in the transfer function. As the case of no eigenvalue multiplicity and using a_p to represent $\sum_{k=p+1}^{p+q}[\frac{\phi_k^{s_i}\phi_k^{a_j}}{M_k}]$ and follow the same procedure, we can still conclude that a_k for $k = 1, \ldots, p, p+q+1, \ldots, n$, should be have the same sign. Even though we only discussed the case of one eigenvalue with multiplicity, if there are other repeated eigenvalues, the conclusion is the same as what stated in this theorem. □

Remark:

1.If any $\frac{\phi_k^{s_i}\phi_k^{a_j}}{M_k}$ or $\sum_{k=p+1}^{p+q}[\frac{\phi_k^{s_i}\phi_k^{a_j}}{M_k}]$ in Equation (38) is equal to zero, pole-zero cancellation occurs for the pole $\mathbf{j}\omega_k$ or $\mathbf{j}\omega_p$

2.For the special case of a collocated actuator and sensor pair, $\phi_k^{s_i} = \phi_k^{a_j}$, for $k = 1, 2, \ldots, n$. The ith condition is obviously satisfied. Therefore, the collocated system always has an alternating pole-zero plot as that of Figure (10).

Finally, we prove the next theorem to guarantee the stability of a PD controller applied to the alternating pole-zero plot of the system in Equation (36).

Theorem 4.3 *The transfer function of Equation (36) has an alternating pole-zero plot if and only if it can be stabilized by a PD controller.*

Proof: The necessary condition of this theorem has already been proved in Theorem 4.1. For the sufficient part, first we formulate the closed loop characteristic equation as,

$$\prod_{k=1}^{n}(s^2 + \omega_k^2) + K_{pd}(s+c)\sum_{k=1}^{n}\left[a_k \prod_{\ell=1,\ell\neq k}^{n}(s^2 + \omega_\ell^2)\right] = 0 \tag{41}$$

where K_{pd} is the gain of the PD controller and $-c < 0$ is the zero introduced by the controller. In addition, the a_k's have the same meaning as in Theorem 4.2. We have already shown in Theorem 4.1 that alternating pole-zero plot will make the angle of departure of all open loop poles pointing to the left hand plane. If we can prove that the root locus of this plot with a PD controller never cross the imaginary axis for any finite gain $|K_{pd}| < \infty$, then the stability is always guaranteed. Assuming the root locus crosses the imaginary axis at $\mathbf{j}\omega$. By substituting $s = \mathbf{j}\omega$ into Equation (41) and equate both the real and imaginary parts to zero, we have,

$$\prod_{k=1}^{n}(-\omega^2+\omega_k^2)+K_{pd}c\sum_{k=1}^{n}\left[a_k\prod_{\ell=1,\ell\neq k}^{n}(-\omega^2+\omega_\ell^2)\right]=0 \tag{42}$$

and

$$K_{pd}\omega\sum_{k=1}^{n}\left[a_k\prod_{\ell=1,\ell\neq k}^{n}(-\omega^2+\omega_\ell^2)\right]=0 \tag{43}$$

Equation (43) is true only when

$$\omega = 0$$

or

$$\sum_{k=1}^{n}\left[a_k\prod_{\ell=1,\ell\neq k}^{n}(-\omega^2+\omega_\ell^2)\right] = 0$$

For the former case, if $\omega = 0$ is substituted into Equation (42), then the equation becomes,

$$\prod_{k=1}^{n}\omega_k^2+K_{pd}c\sum_{k=1}^{n}a_k\prod_{\ell=1,\ell\neq k}^{n}\omega_\ell^2=0$$

Since all a_k's have the same sign and if a K_{pd} of suitable sign is used, the equation can never be equal to zero. Therefore, 0 is not on the root locus. In the latter case, the solution of ω corresponds to the open loop zeros of the system. Then the equation is substituted into Equation (42) again. Equation (42) is true only when $K_{pd} = \infty$ or $K_{pd} = -\infty$ with the sign dependent on the sign of the a_k's. This is due to the fact if finite value of K_{pd} is used, the first term of Equation (42) becomes zero while the second term is nonzero because of the alternating pole-zero plot (the open loop zeros can never be equal to the open loop poles). From above argument we have proved that the alternating pole-zero plot can always be stabilized by PD controller, which is the sufficient condition of this theorem. □

In order to apply the above theorem and illustrate the consequence of a given actuator/sensor system configuration, we consider only the first vibration mode. Because the first three modes correspond to the rigid body motion with eigenvalue equal to zero, it can be shown from Theorem 4.2 that the transfer function between the *ith* input and *jth* output will have an alternating pole-zero plot if and only

$$\begin{aligned}&(i)\quad \left(\frac{\phi_1^{a_i}\phi_1^{a_j}}{M_1}+\frac{\phi_2^{a_i}\phi_2^{a_j}}{M_2}+\frac{\phi_3^{a_i}\phi_3^{a_j}}{M_3}\right)\geq 0\\ &(ii)\quad \frac{\phi_4^{a_i}\phi_4^{a_j}}{M_4}\geq 0\end{aligned} \tag{44}$$

or

$$\begin{aligned}&(i)\quad \left(\frac{\phi_1^{a_i}\phi_1^{a_j}}{M_1}+\frac{\phi_2^{a_i}\phi_2^{a_j}}{M_2}+\frac{\phi_3^{a_i}\phi_3^{a_j}}{M_3}\right)\leq 0\\ &(ii)\quad \frac{\phi_4^{a_i}\phi_4^{a_j}}{M_4}\leq 0\end{aligned} \tag{45}$$

In order to gain more insight, the mode shape functions obtained from the Rayleigh-Ritz method are substituted in the above equations. Consider the case of a rectangle plate, if the length-to-width ratio $\frac{a}{b}$ is between 0.65 and 1.54, the first four mode shape functions can be calculated as $\phi_1(x,y) = 1$, $\phi_2(x,y) = f_{b_2}(y)$, $\phi_3(x,y) = f_{a_2}(x)$, $\phi_4(x,y) = f_{a_2}(x)f_{b_2}(y)$ and $M_1 = M_2 = M_3 = M_4$. If they are substituted, Equation (44) and (45) can be rearranged as,

$$\begin{aligned}&(i)\quad \frac{1}{12}+\left[\frac{1}{a}(x_{s_i}-\frac{a}{2}),\frac{1}{b}(y_{s_i}-\frac{b}{2})\right]\left[\frac{1}{a}((x_{a_j}-\frac{a}{2}),\frac{1}{b}(y_{a_j}-\frac{b}{2})\right]\geq 0\\ &(ii)\quad \left(\frac{a}{2}-x_{s_i}\right)\left(\frac{a}{2}-x_{a_j}\right)\left(\frac{b}{2}-y_{s_i}\right)\left(\frac{b}{2}-y_{a_j}\right)\geq 0\end{aligned} \tag{46}$$

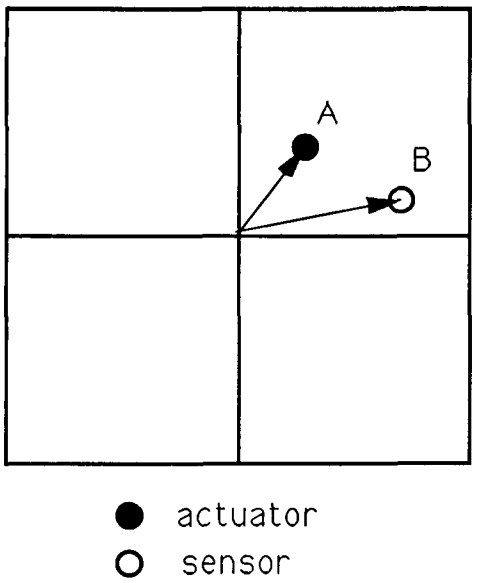

Figure 11: Case 1 for locating the actuator and sensor to achieve desirable alternating pole-zero type

and

$$\begin{aligned} &(i) \quad \tfrac{1}{12} + \left[\tfrac{1}{a}(x_{s_i} - \tfrac{a}{2}), \tfrac{1}{b}(y_{s_i} - \tfrac{b}{2})\right] \left[\tfrac{1}{a}((x_{a_j} - \tfrac{a}{2}), \tfrac{1}{b}(y_{a_j} - \tfrac{b}{2})\right] \leq 0 \\ &(ii) \qquad \left(\tfrac{a}{2} - x_{s_i}\right) \left(\tfrac{a}{2} - x_{a_j}\right) \left(\tfrac{b}{2} - y_{s_i}\right) \left(\tfrac{b}{2} - y_{a_j}\right) \leq 0 \end{aligned} \tag{47}$$

Conditions (i) of Equation (46) and (47) can be interpreted geometrically as comparing $\frac{1}{12}$ with the inner product of two vectors. These two vectors have starting points at the center of the plate and end points at the locations at the actuator or sensor, but their x and y components are normalized with respect to a and b individually. If the rectangle plate are divided into four quadrants by the lines $x = \frac{a}{2}$ and $y = \frac{b}{2}$, then condition (ii) of Equation (46) is satisfied if the actuator and sensor are in the same quadrant or they are in opposite quadrant individually. However, condition (ii) of Equation (47) is satisfied if the actuator and sensor are in the adjacent quadrants individually. Therefore, for the transfer function to have an alternating pole-zero plot , there are basically three ways to locate the actuator and sensor. These three cases are described below.

- Case 1 : Locate actuator and sensor in the same quadrant as shown in Figure (11). Condition (i) of Equation (46) is satisfied automatically because the inner product of the two normalized vectors are always greater than zero. If either the actuator or sensor is located at the node lines of $\phi_4(x, y)$ which are composed of the lines $x = \frac{a}{2}$ and $y = \frac{b}{2}$, then the zeros cancel the two poles symmetrically on the imaginary axis and there are only two poles at the origin.
- Case 2 : Locate actuator and sensor in the opposite quadrants individually and check if condition (i) of Equation (46) is satisfied. For the special case of a square plate as shown in Figure (12), if the sum of $\frac{a^2}{12}$ and the inner porduct of vectors $\vec{OA}$ and $\vec{OB}$ is greater than 0, then the condition is satisfied. Also when the sum is equal to zero, then the zeros cancel the two poles at the origin and there are only two poles symmetrically on the imaginary axis.

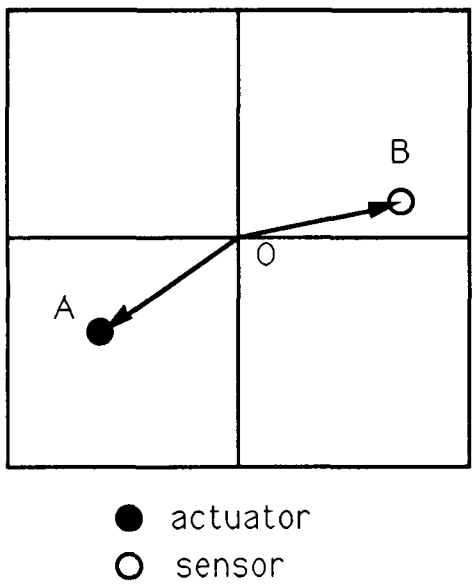

Figure 12: Case 2 for locating the actuator and sensor to achieve desirable alternating pole-zero type

- Case 3 : Locate actuator and sensor in the adjacent quadrants individually and check if condition (i) of Equation (47) is satisfied. By the same argument in case 2, if the plate is square, the sum of $\frac{a^2}{12}$ and the inner product of vectors $\vec{OA}$ and $\vec{OB}$ of Figure (13) should be less than 0. One obvious result is that the angle between the two vectors has to be greater than 90 degrees. Also as in case 2, when the sum is equal to zero, then the zeros cancel the two poles at the origin and there are only two poles symmetrically on the imaginary axis.

5 Effects of Damping

In the above discussion, we assume that there is no energy dissipation or system damping in the vibration of a flexible plate. But damping normally exist in the physical systems. Especially in the vibration isolation table, damping is a favorable effect because with proper damping mechanism (e.g. viscoelastic material), the higher frequency vibrations that reach the table top can be attenuated rapidly.

For the case of weak damping effects, it can be guaranteed that the controllability and observability conditions obtained in Section 3 are still acceptable. This is because the controllability and observability are preserved under sufficient small perturbation such as the damping effect [15, 16]. However, when the damping is not negligible, the modes will couple with each other. Therefore, certain modes originally uncontrollable (unobservable) in the case of no damping may become controllable (observable) [6]. If the system damping is sufficiently large. It is also pointed out in [6] that the number of actuators (sensors) to achieve controllability (observability) are expected to be reduced because of the significant coupling effect.

On the other hand, the influences of damping on the system pole-zero plot is that the open loop poles are now placed in the left hand plane instead of being on the imaginary axis. The larger the damping, the further the poles are from the imaginary axis. Therefore damping tends to stabilize

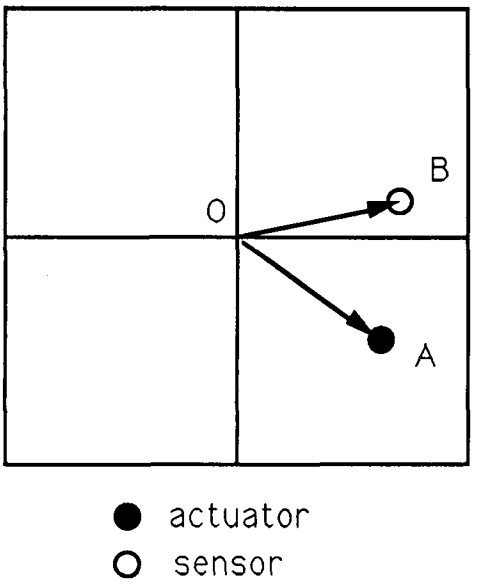

Figure 13: Case 3 for locating the actuator and sensor to achieve desirable alternating pole-zero type

the overall system and make the controller easier to implement.

6 Conclusion

This paper investigated the relationships between actuator and sensor locations and the dynamics and control characteristics of a magnetically levitated vibration isolation system. The problem was formulated using orthogonal mode shape functions based on the Rayleigh-Ritz method. A lumped-parameter model of a flexible vibration isolation table top is used to investigate the system's controllability and observability including the coupling effects introduced by by the magnetic bearing. The selection of proper actuator and sensor locations leading to a controllable and observable system were discussed. Necessary and sufficient conditions were derived for proper selection of actuator and sensor locations, and for reducing the controller complexity. The results are illustrated by examples using approximate mode shape functions. Such information is important for the overall design of ultra high performance vibration isolation systems.

A Rayleigh-Ritz method

Assuming that the plate is vibrating with a mode shape $\phi(x,y)$ and frequency ω , the Rayleigh-Ritz method proceeds by calculating the maximum potential energy from Equation (6),

$$\mathcal{V}_{max} = \frac{D}{2}\int_A [\phi_{xx}^2 + \phi_{yy}^2 + 2\nu\phi_{xx}\phi_{yy} + 2(1-\nu)(\phi_{xy})^2]dA \tag{48}$$

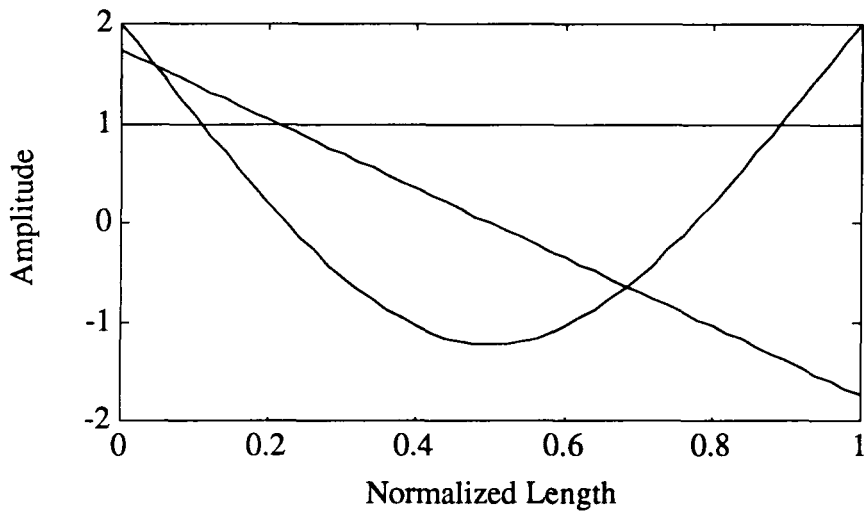

Figure 14: The first three modeshape functions of prismatic beam with free ends

Also the maximum kinetic energy from Equation (5) is given by,

$$\mathcal{T}_{max} = \frac{D}{2}\rho h\omega^2 \int_A \phi^2 dA \tag{49}$$

By equating the above two equations, an expression for the frequency ω is obtained,

$$\omega^2 = \frac{\rho h}{2} \frac{\mathcal{V}_{max}}{\int_A \phi^2 dA} \tag{50}$$

The Rayleigh-Ritz method assumes that the mode shape functions can be expanded by a linear series of "admissible" functions and adjusts the coefficients in the series to minimize Equation (50). For the case of rectangle plate with length a and width b, the mode shape function $\phi(x,y)$ is expanded as :

$$\phi(x,y) = \sum_{n=1}^{3}\sum_{m=1}^{3} A_{mn} f_{a_m}(x) f_{b_n}(y) \tag{51}$$

where the function $f_{\beta_i}(.)$ is the ith mode shape function of a prismatic beam with free ends and length β. The first three mode shape functions are plotted in Figure 14. We can write these first three modeshape functions as : $f_{\beta_1}(\xi) = 1$, $f_{\beta_2}(\xi) = \sqrt{3}(1-\frac{2\xi}{\beta})$, $f_{\beta_3}(\xi) = cosh(\frac{4.73\xi}{\beta}) - cos(\frac{4.73\xi}{\beta}) - 0.983[sinh(\frac{4.73\xi}{\beta}) - sin(\frac{4.73\xi}{\beta})]$. By substituting these into Equation (51), Equation (50) becomes a function of A_{mn} . Then we minimize it by taking the partial derivative with respect to each coefficient and equating to zero then follow the same procedure as in [17], we arrive at a set of equations each of which has the form,

$$\sum_{n=1}^{3}\sum_{m=1}^{3} [C_{mn}^{(ik)} - \lambda\delta_{mn}] A_{mn} = 0 \tag{52}$$

where

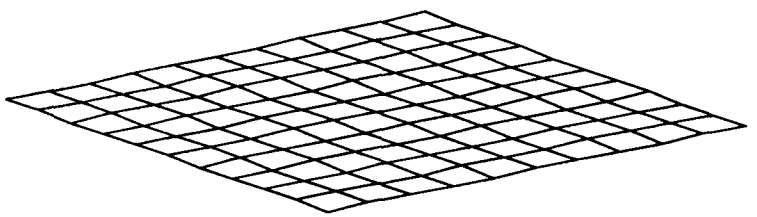

Figure 15: The 1st mode with normalized frequency 0

$$C_{mn}^{(ik)} = \nu\frac{a}{b}[E_{mi}E_{kn} + E_{im}E_{nk}] + 2(1-\nu)\frac{a}{b}H_{im}H_{kn}, \quad \delta_{mn} = 1, \quad \text{for } mn \neq ik$$

$$C_{mn}^{(ik)} = \frac{b}{a}\epsilon_i^4 + \frac{a^3}{b^3}\epsilon_k^4 + 2\nu\frac{a}{b}E_{ii}F_{kk} + 2(1-\nu)\frac{a}{b}H_{ii}H_{kk}, \quad \delta_{mn} = 1, \quad \text{for } mn = ik$$

and

$$E_{im} = \beta\int_0^\beta f_{\beta_i}(\xi)\frac{d^2 f_{\beta_m}(\xi)}{d\xi^2}d\xi, \quad H_{im} = \beta\int_0^\beta \frac{df_{\beta_i}(\xi)}{d\xi}\frac{df_{\beta_m}(\xi)}{d\xi}d\xi, \quad \epsilon_1 = \epsilon_2 = 0, \epsilon_3 = 4.730$$

The above set of linear equations is a typical eigenvalue problem in linear algebra. In this paper, we take the Poisson ratio ν as 0.3 and solve Equation (52) using the Matlab package and thus get nine approximate mode shape functions and corresponding normalized natural frequencies. For the special case of square plate, the nine mode shape functions and corresponding normalized natural frequencies were computed using Matlab and found to be,

$$\begin{array}{ll}
\omega_1^* = 0 & \phi_1(x,y) = 1 \\
\omega_2^* = 0 & \phi_2(x,y) = f_2(y) \\
\omega_3^* = 0 & \phi_3(x,y) = f_2(x) \\
\omega_4^* = 14.07 & \phi_4(x,y) = f_2(x)f_2(y) \\
\omega_5^* = 19.01 & \phi_5(x,y) = 0.7071f_3(y) - 0.7071f_3(x) \\
\omega_6^* = 24.62 & \phi_6(x,y) = 0.7069f_3(y) + 0.7069f_3(x) + 0.0262f_3(x)f_3(y) \\
\omega_7^* = 32.69 & \phi_7(x,y) = f_2(x)f_3(y) \\
\omega_8^* = 32.69 & \phi_8(x,y) = f_3(x)f_2(y) \\
\omega_9^* = 66.82 & \phi_9(x,y) = -0.0185f_3(y) - 0.0185f_2(x) + 0.9497f_3(x)f_3(y)
\end{array} \tag{53}$$

where the normalized frequency $\omega^* = \frac{\omega a^2}{h}\sqrt{\frac{12\rho(1-\nu^2)}{E}}$ and $f_j(\xi) = f_{\beta_j}(\xi)$ as appeared in the appendix. Figure 15 to Figure 23 are the 3-D approximate modeshape functions of square plate.

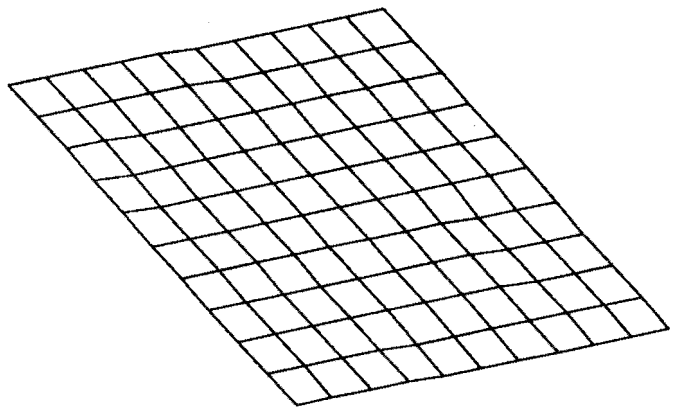

Figure 16: The 2nd mode with normalized frequency 0

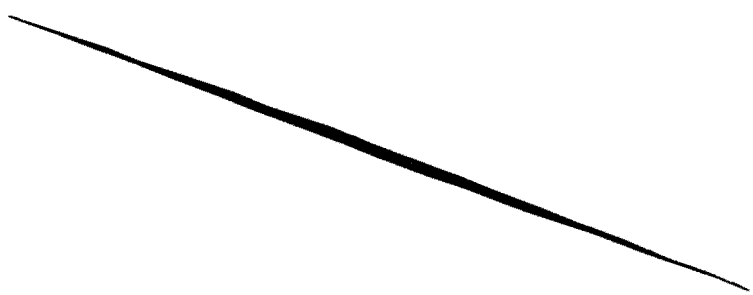

Figure 17: The 3rd mode with normalized frequency 0

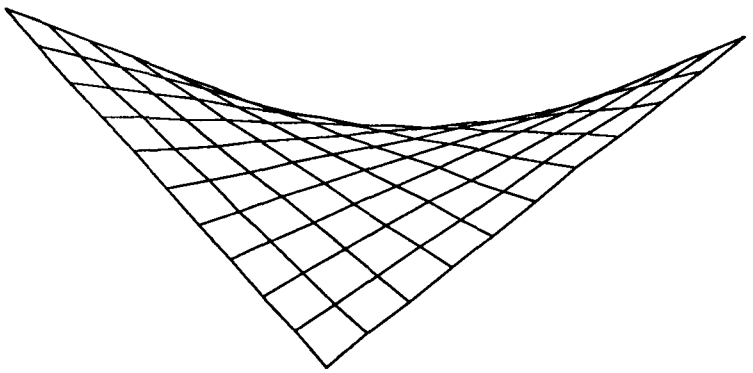

Figure 18: The 4th mode with normalized frequency 14.07

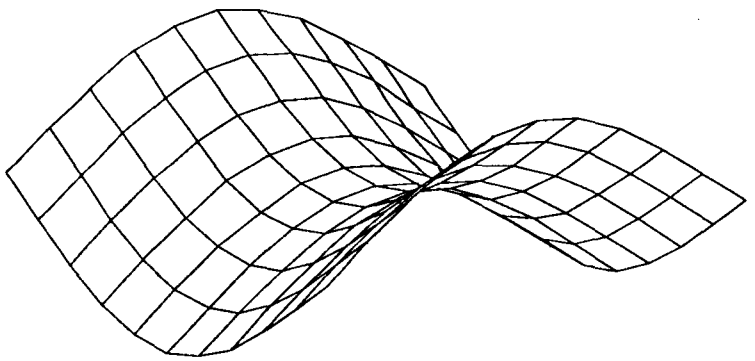

Figure 19: The 5th mode with normalized frequency 19.81

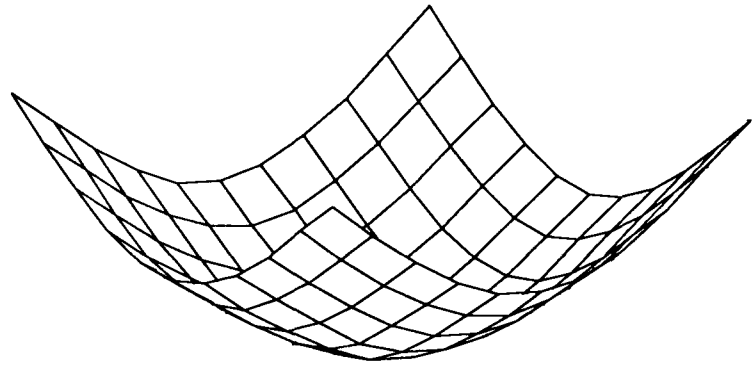

Figure 20: The 6th mode with normalized frequency 24.62

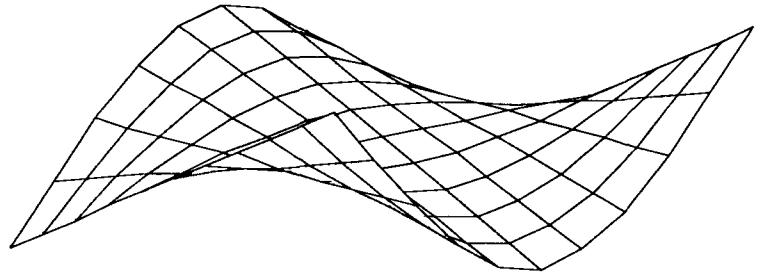

Figure 21: The 7th mode with normalized frequency 36.29

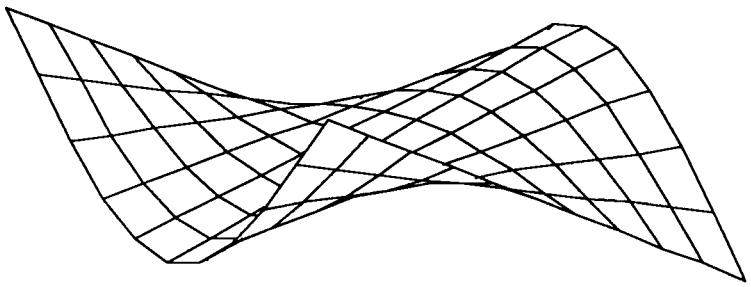

Figure 22: The 8th mode with normalized frequency 36.29

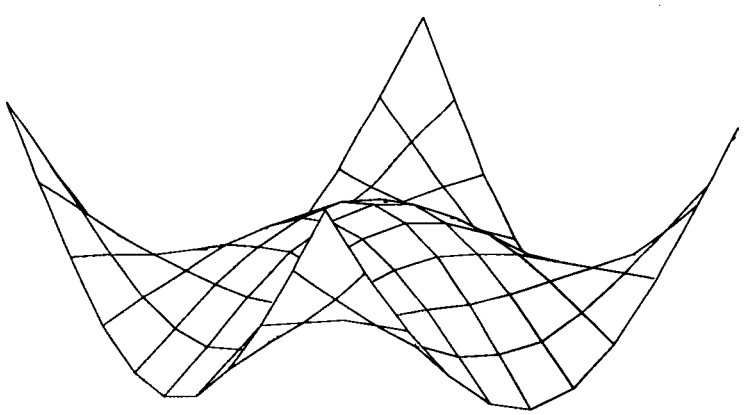

Figure 23: The 9th mode with normalized frequency 66.82

References

[1] Slocum, A., *Precision Machine Design*, Draft, 1989.

[2] Binnig, G., and Rohrer, H., "Scanning Tunneling Microscopy," Helvetica Physica Acta, Vol. 55, 1982, pp. 726–735.

[3] Harris, C. M. and Crede, C. E., *Shock and Vibration Handbook*, McGraw-Hill Book Company, New York 1976.

[4] Sandercock, J. R., "A Dynamic Antivibration System," Proceedings of First International Conference of Vibration control in Optics and Metrology, February 1987, London, England, pp. 157–165.

[5] Newport Catalog in, "Vibration Isolation System," CA, 1990.

[6] Hughes, P. C. and Skelton, R. E., "Controllability and Observability of Linear Matrix-Second-Order Systems," Journal of Applied Mechanics, Vol. 47, June 1980, pp. 415–420.

[7] Yang, B. and Mote, C. D. Jr., "Controllability and Observability of Distributed Gyroscopic Systems," Journal of Dynamic Systems, Measurement, and Control, Vol. 113, March 1991, pp. 11–17.

[8] Park, J-H and Asada, H., "Design and Control of Minimum-Phase Flexible Arms with Torque Transmission Mechanisms," IEEE International Conference on Robotics and Automation, May 1990, pp. 1790–1795.

[9] Bennighof, J. K. and Meirovitch, L., "Active Vibration of a Distributed System With Moving Support," Journal of Vibration, Acoustics, Stress, and Reliability in Design, Vol. 110, 1988, pp. 246–253.

[10] Timoshenko, S., *Theory of Plates and Shells*, McGraw-Hall Book Company, Inc., New York and London, 1940.

[11] Soedel, W., *Vibrations of Shells and Plates*, Marcel Dekker, Inc. New York and Basel, 1982.

[12] Chen, C-T, *Linear System Theory and Design*, Holt, Rinehart and Winston, 1984.

[13] Timoshenko, S. and Young, D. H., *Vibration Problems in Engineering*, New York, Van Nostrand, 1975.

[14] Ogata, K., *Modern Control Engineering*, Prentice-Hall Inc. 1990.

[15] Balas, M. J., "Feedback Control of Flexible Systems," IEEE Trans. Automatic Control, Vol. AC-23, Aug. 1978, pp. 674–679.

[16] Wonham, W., *Multivariable Control*, Springer, 1974.

[17] Young, D., "Vibration of Rectangular Plates By the Ritz Method," Journal of Applied Mechanics, 17, 1950, pp. 448–453.

Bibliography

[1] Hisatani, M., Inami, S., Ohtsuka, T. and Fujita, M., "Design and Testing of a Flexible Rotor-Magnetic Bearing System," Proceedings of the Second International Symposium on Magnetic Bearings, July 1990, Tokyo, Japan, pp. 131–138.

[2] McCallum, D. C., "Dynamic Modelling and Analysis of a Magnetically Suspended Flexible Rotor," NASA Conference in Aerospace Applications of Magnetic Suspension Technology, September 1990, pp. 499–538.

[3] Meirovitch, L., *Analytical Methods in Vibrations*, The Macmillan Co., New York, 1967.